Topological conditions of gene regulatory networks enabling robust binary cell-fate decision-making

Running title: Topological analysis of binary cell-fate networks

Sai Shyam[1], Nikhil Nandan[1], Mohit Kumar Jolly[1,*], Kishore Hari[1,2,*]

[1] Department of Bioengineering, Indian Institute of Science, Bangalore, 560012, India

[2] Current address: Centre for Theoretical Biological Physics, Northeastern University, MA 02115, USA

*Authors to whom correspondence may be addressed:
mkjolly@iisc.ac.in (M.K.J.), a.hari@northeastern.edu (K.H.)

Abstract

Embryonic development entails multi-layer branching of cell-fate decision processes; often, each branch corresponding to a binary cell-fate decision. The two phenotypes at such branching points usually have mutually exclusive gene expression patterns, driven by two master regulators that mutually inhibit each other and can activate themselves, forming a toggle switch. The dynamics of a toggle switch have been extensively studied, however, the regulatory networks underlying cell-fate decision often involve many transcription factors. We recently showed that these networks can be organized as two mutually inhibiting “teams of nodes”, such that the nodes of the same team predominantly activate themselves, while those of the opposite teams primarily inhibit each other. While the ideal cases of fully connected and consistent networks of two “teams of nodes” have been well-understood, a detailed understanding of the effect of varying levels of connectivity and inconsistency in the edges with respect to the configuration of teams is lacking. Here, we simulate networks of two-teams (TTN) under varying degrees of edge density, edge impurity and external influence to identify the conditions under which these networks can give rise to a robust binary cell-fate decision system. We find that the emergent cell-fate decision landscape is much more sensitive to inconsistent edges than to low connectivity, and that TTN generally lead to a more robust landscape than a toggle switch in the context of buffering external perturbations. Our results offer insights into the design principles of gene regulatory networks engaged in binary cell-fate decisions and can be extended to evaluate strategies for cellular reprogramming.

Keywords

Cell-fate decisions; Gene Regulatory Networks; Toggle Switch; Network analysis; Multistability

Introduction

Phenotypic plasticity, the ability of cells to change their phenotypes reversibly in response to changing environments, is a fundamental phenomenon (Mills et al. 2019) across different contexts including embryonic development and disease (Jopling et al. 2011; Gupta et al. 2019; Kalra et al. 2021; Pérez-González et al. 2023). It is driven by changes in expression patterns of biochemical molecules and is often understood by studying the underlying gene regulatory networks (GRNs). Many embryonic cell-fate decisions have been shown to be governed by relative expression levels of two mutually repressing genes (Zhou and Huang 2011). This regulatory motif of two genes (A and B) mutually inhibiting each other is called a Toggle Switch (TS) and can give rise to two co-existing stable steady states that can switch back and forth: (high A, low B) and (low A, high B) (Gardner et al. 2000). For example, the master regulator genes PU.1 and GATA1 form a toggle switch that influences the differentiation of common myeloid progenitor cells into myeloid and erythroid progenitors based on the relative expression of these two genes. (High PU.1, low GATA1) facilitates the differentiation of the common myeloid progenitor cell into myeloid cells, while (low PU.1, high GATA1) leads to differentiation into erythroid cells. A third state, enabled by self-activation on the two transcription factors, has a balanced expression level of both PU.1 and GATA1 molecules and corresponds to the progenitor state (Roeder and Glauche 2006). Similar binary cell-fate decision systems are also important in cancer (Pérez-González et al., 2023; Sahoo et al., 2021). A prime example is epithelial-to-mesenchymal transition (EMT), where a toggle switch between the family of transcription factors ZEB1/2 and the family of miR-200 microRNAs has been identified to be a core motif in the underlying GRNs(Brabletz and Brabletz 2010; Celià-Terrassa et al. 2018). The self-activation of ZEB1 supports the emergence of a hybrid E/M state, composed of expression of both ZEB1/2 and miR200 molecules similar to the progenitor state in the (PU.1, GATA1) example (Lu et al. 2013; Jolly et al. 2018). These hybrid E/M states have been shown to be more stem-like, drug resistant and metastatically fit (Pastushenko and Blanpain 2019).

The dynamics of a toggle switch including transcription factors and/or microRNAs have been well-studied using deterministic and stochastic models to capture qualitative features of binary cell-fate decisions(Tian and Burrage 2006; Roeder and Glauche 2006; Shiraishi et al. 2010; Jaruszewicz and Lipniacki 2013; Okawa et al. 2016). However, across different contexts, the underlying GRNs of cell-fate decisions are larger in size encompassing multiple toggle switches and feedback loops (Ríos et al. 2015; Udyavar et al. 2017; Hari et al. 2020; Arthur et al. 2024). Recently, we analysed the networks governing EMT and found the presence of two teams of nodes (Hari et al. 2022b). A team is a group of genes that activate member genes belonging to the same team while inhibiting genes of other teams directly and/or indirectly. For instance, in the EMT network, most members in epithelial team members were EMT-inhibiting microRNAs such as miR-200 family while most members in mesenchymal team were EMT-inducing transcription factors (EMT-TFs) such as ZEB1 and SNAI1. Many of these EMT-TFs activated each other and also repressed microRNAs that targeted them or other EMT-TFs, while many microRNAs inhibited EMT-TFs that inhibited them or other microRNAs in the same team. By showing the presence of teams in different gene regulatory networks reported in EMT, we proposed that ‘teams’ could serve as general design principles for the regulation of robust, bimodal phenotypic landscape. Such ‘teams’ were seen across other biological contexts as well, including developmental decision-making (Chauhan et al. 2021; Pillai and Jolly 2021; Sehgal et al. 2024; Hari et al. 2025). However, a detailed understanding of how network parameters internal to the network of genes forming such ‘teams’ genes and interactions with other network nodes within

which such ‘teams’ may be embedded has not yet been elucidated. Thus, their impact on the phenotypic repertoire of decision-making GRNs remains to be elusive.

Here, we investigated the effect of topological properties of two-team networks (TTNs) on the resultant phenotypic landscape enabled by GRNs. We simulated TTNs and the toggle switch using two simulation formalisms : RACIPE, a continuous state-space, ODE-based simulation formalism that calculates network dynamics over a large parameter space (Huang et al. 2018), and a threshold based Boolean formalism, a discrete state-space approach that considers only the effect of the network topology without any parameter sets(Font-Clos et al. 2018). We used the toggle switch as a reference to elucidate the conditions under which a TTN can be approximated to a simple toggle switch. We studied the properties of isolated TTNs and the TTNs embedded in larger GRNs and compare the emergent phenotypic landscape with that of a toggle switch. We focused on two properties of the phenotypic landscape: a) the frequency of ‘pure states’ emergent from the network (F1) (i.e. frequency of the mutually exclusive states where one ‘team’ is “on” and the other ‘team’ is “off”) and b) the correlation between the expression levels of the nodes belonging to two teams (CC). We demonstrated that, despite structural similarities between a TTN and a toggle switch, even the fundamental properties such F1 and CC vary widely dependent on the density and impurity present in the TTN. Further, we found that TTNs are more resilient as compared to a toggle switch, when embedded in larger networks, thus enabling robust cellular decision-making.

Results

High density two-team networks have similar properties as a toggle switch

A toggle switch between A and B **(Fig 1A)** allows coexistence of two states: 10 (A high, B low) and 01 (A low, B high) (Gardner et al. 2000). Boolean simulations of a toggle switch (TS) without self-activations result only in 01 and 10 as steady states, while the addition of self-activation allows for the hybrid state (11 and 00 states) as well (Hari et al. 2022a). For ODE-based simulations of a toggle switch using RACIPE, a majority of parameter sets converges to these two steady states (Huang et al. 2017). These two mutually exclusive states often represent two cell fates in a network model describing the events of cellular differentiation. We recently identified that certain larger networks describing cell-fate decisions can be approximated as two mutually inhibiting “teams” of nodes such that members in a team effectively activate each other while those across teams inhibit each other. Thus, members in a “team” can work together as a single unit – a “hypernode” – leading to properties qualitatively similar to that of toggle switch.

Here, we simulate the TTNs as well as toggle switch networks using RACIPE(Huang et al. 2018) and Boolean formalisms(Font-Clos et al. 2018) and quantify the differences between TS **(Fig 1B)** and TTNs **(Fig 1C)** using two metrics: F1 - the total frequency of “pure” phenotypes (where all the nodes of one team have high expression and all those of the other team have low expression, equivalent to 10 or 01 states in TS) and CC – the strength of correlation between the “teams” (see methods). We study the effect of three parameters in TTN networks on F1 and CC: 1) Network size (number of nodes in a network, ranging from 4 to 40), 2) Density (percentage of edges present in the network, ranges from 20% to 100%) and 3) Impurity (percentage of edges conflicting with the “team” configuration, ranges from 0% to 100%). Note that we refer to density and impurity as “Core Edge Density” and “Core Edge Impurity”, where core edges refer to edges within the TTN. We use this terminology to differentiate the properties of core network from the peripheral/external network later in the embedding simulations done later. described in **Fig 5**. We

generated multiple such bootstrapped networks for each combination of the above parameters explored, using the stochastic block model with constant probability for each community (Holland et al. 1983). For symmetry, we maintained both the teams with the same number of nodes (N/2), where N is number of nodes in the network (see Methods for detailed protocol to generate these networks).

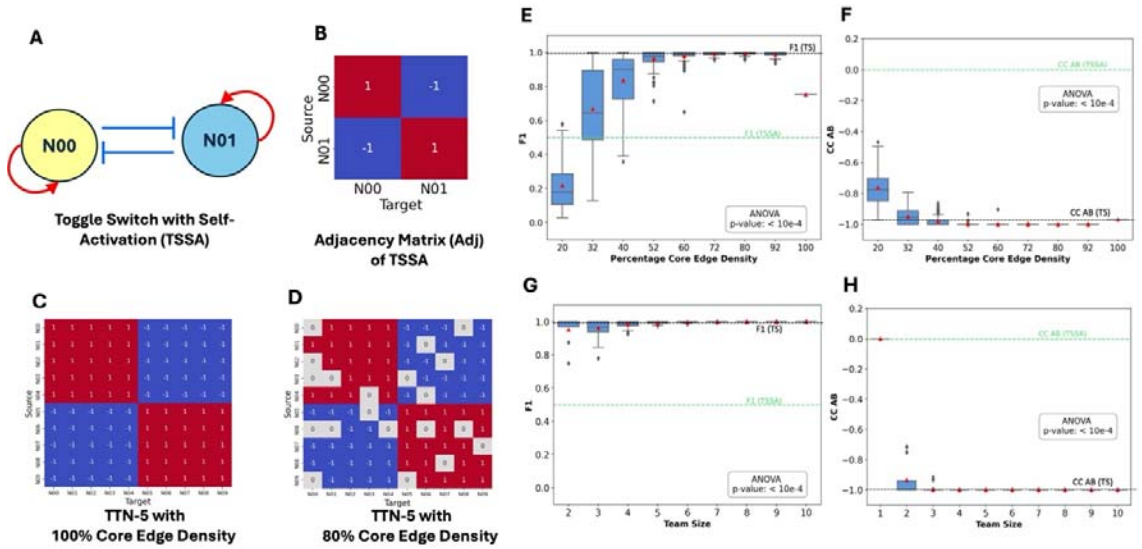

***Figure 1: F1 and CC AB as a function of the edge density in two-team networks (TTNs)**. **A)** Toggle Switch with Self Activation (TSSA): Motif comprised of two genes N00 and N01, showing mutual inhibition between two self-activating nodes. **B)** Adjacency Matrix representing the interactions of the TSSA. Adjacency Matrix for a TTN of Size 5 and **C)** 100% Core Edge Density, **D)** 80% Edge Density. Comparison between distributions of F1 with Variation in **E)** Percentage Edge Density and **G)** Team Size. Comparison between distributions of CC AB with Variation in **F)** Percentage Edge Density and **H)** Team Size. Results of 1-way ANOVA indicated on the plot.*

We previously demonstrated that increasing core edge density leads to strong teams and a low-dimensional phenotypic space (Hari et al. 2025). Hence, we first explored the effect of density on F1 and CC by generating some networks with different density values, without considering any impurity in the network **(Fig 1D)**. As expected, we find that the fraction of 'pure' (mutually exclusive) states increases with increasing density in both Boolean and continuous simulations (**Fig1E, S1A**). At low densities, TTN has mean F1 values around 0.2 and reach their corresponding maximum values in both simulation formalisms at around 60% density. In Boolean simulations, the maximum value of F1 is 1 and in continuous simulations it is around 0.85. In both cases, the maximum F1 of TTN networks is equal to or above the F1 values obtained from a TS (as shown by the horizontal lines). Interestingly, at densities greater than 90% in both Boolean and continuous simulations, F1 values decreased to around 0.8. This observation is analogous to the increase in the frequency of hybrid states in TSSA as compared to TS (Hari et al. 2022a). Consistently, we find that the fraction of pure states in a two-node toggle switch with self-activations (TSSA) is lower than that of TS (horizontal lines in **Fig 1C-D**). Up to 90% density, the activations within teams contribute towards making the teams work as single entities, beyond which the activation links within a team amount to adding a self-activation to the super-nodes, thereby increasing the occurrence of "hybrid" phenotypes. To further understand this behaviour, we removed all activation links from the TTN networks and found that F1 monotonically increased with density (**Fig S1B, C)**.

The correlation coefficients of TTN networks remained strongly negative. At lower densities (20%), CC AB shows a higher variance. As the density increases, the variance decreases, with the mean approaching that of TS in both Boolean and continuous simulations **(Fig 1F, S1C)**. Thus, TTN at any density can be simplified as a TS while studying the correlation between expression of teams/phenotypes. For the more nuanced studies involving the fraction of pure states in a population governed by these networks, tacitly simplifying TTN to TS or TSSA is not always valid. We further explored the effect of team size on F1 and CC. At 80% density, We find that while small sized networks have lower values of F1, F1 values reach 1 after team size 4 and have minor fluctuations afterwards **(Fig 1G, H, S1D)**. F1 and CC AB do show a dependence on the team size at 20% density (**Fig S1E,F)**. As the team size increases from 5 to 10, the F1 value increases at 20% density with the mean F1 reaching 0.8, and CC AB reaches -1. At other density values, however, team size does not seem to have a significant effect on the phenotypic landscape.

Impurities in TTN reduce the frequency of 'pure states' as seen in toggle switch

Not every GRN can be approximated as a high-density TTN effectively. Besides being moderately dense, biological networks also consist of some edges that may appear like impurities in the context of 'team' behaviour, such as auto-inhibitory feedback loops (for instance, seen in SNAIL1(Peiró et al. 2006)) and incoherent feedforward loops(Lai et al. 2016), or mutual inhibition between EMT-TFs such as SNAIl1 and SNAI2 (Subbalakshmi et al. 2022) or that between ZEB1 and ZEB2 (Vandamme et al. 2020). These structures play a crucial role in the contexts of robustness, noise dynamics and signal transmission (Cinquin and Demongeot 2002; Dublanche et al. 2006; Zhang et al. 2012). Quantifying the effect of these inconsistent links can be challenging. The 'teams' conceptualization provides us with a way to quantify the extent of such inconsistencies. In a TTN structure, the interactions among nodes belonging to the same team should be activating (if present) and the interactions among nodes belonging to opposite teams should be inhibiting (if present). Presence of inconsistencies allows for negative interactions within teams and/or positive interactions across. We refer to the fraction of such inconsistent interactions in a TTN as the impurity of the network.

Frustration of a steady state, a metric that measures the extent of inconsistency between the configuration of a steady state and the network topology, correlates negatively with the frequency of the steady state(Tripathi et al. 2020; Hari et al. 2022b). An activatory (inhibitory) edge is frustrated if the expression levels of the nodes corresponding to the edge do not have the same expression level (have the same expression level). Frustration of a state is defined as the fraction of such frustrated edges. In the absence of impurities, the 'pure' states (111110000 or 000011111 for a 10-node TTN) are not frustrated. However, as we introduce impurities in a TTN, the 'pure states' of the original TTNs become frustrated with the value of frustration equal to the fraction of impure edges in the network. Given the previously observed negative correlation between frustration and steady state frequency, we predict the F1 metric to decrease as the number of impurities increase in the network. To test this prediction, we introduced different fractions of impure edges in networks having maximum F1 (80% density) and calculated the effect of impurity on the F1 and CC measures **(Fig 2A)**. We find that impurities strongly effect F1 for both Boolean and continuous simulation formalisms **(Fig 2B,C,S2B, C)**. The mean F1 reduced from 1 at 0% impurity to 0.65 at an impurity value of 20% and to 0 at 40% **(Fig 2B)**. F1 is defined as the frequency of 'pure states', that is, for TTN with 5 nodes per team, either 1111100000 or 0000011111 are the only states acceptable under F1 calculation. States that deviate even by one

node, such as 1111100100, are not counted in F1. This strict definition of F1 can explain the sharp decrease in F1 frequency with increase in impurity. We then relaxed the definition of F1 by including the frequency of states with deviation from pure states up to one and two nodes (**Fig S2D),** thereby creating two relaxed F1 metrics. While the mean values of these relaxed F1 metrics are larger than that of the strict F1, we still see a sudden decrease in the mean values of these metrics from 20% to 40% impurity. A subset of networks do show higher values of the relaxed metrics as well as the strict F1, suggesting the existence of additional network features that can regulate the effect of impurity on F1. From 60% impurity onwards, both the relaxed F1 metrics have zero values as well.

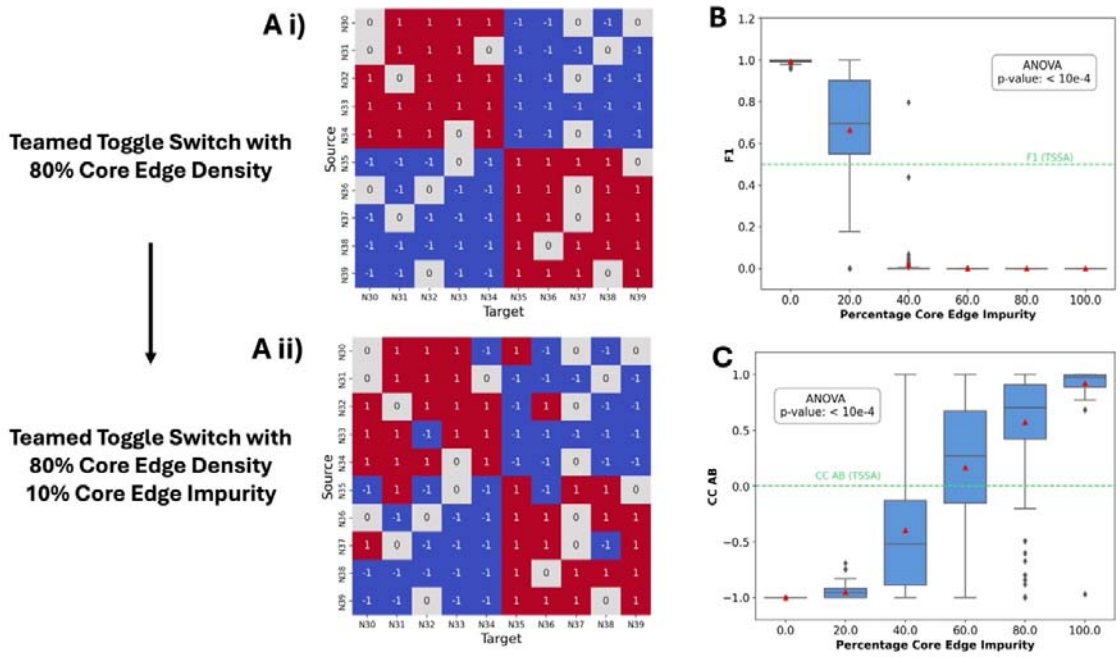

Figure 2: Impurities in TTN reduce F1 and increase CC. A) *Schematic showing the procedure followed to introduce impurity into a TTS Core, by flip Pure Edges to Impure Edges. A pure edge in the adjacency matrix is an activating interaction between genes of the same team or an inhibitory interaction between genes of the opposite team.* ***A, i)*** *Adjacency Matrix of a TTS-5 Core having 80% Edge Density,* ***A,ii)*** *Adjacency Matrix TTS-5 Core in (Ai) upon introducing 10% Impurity. Comparison between distributions of CC AB* ***(B)*** *and F1* ***(C)*** *with Variation in Percentage Core Edge Impurity. Red triangle in each box indicates the mean value of the distribution. Results of 1-way ANOVA indicated on the plot.*

CC AB provides a better understanding of the changes in the phenotypic landscape as compared to F1 with changing impurity. The mean correlation strength between the two teams reduces as impurities are introduced, nearing zero as the impurities reach 50%. With further increase in impurities, the correlation coefficient changes sign from negative to positive and starts increasing, reaching 1 at 100% impurity **(Fig 2D)**. At 100% impurity, the TTN is effectively no longer a mutually inhibiting teams case, but a mutually activating one, thus leading to strong positive correlation. Correspondingly, we see the frequency of states with both teams “on” or both teams “off” increase with higher impurity **(Fig S2E).** Similar to F1, at 20% impurity, more than 75% of the networks show a stronger correlation than TSSA, but most networks have a weaker correlation than TS (-1). At 60% impurity, a significant fraction of the networks (>25%) still showed negative CC AB. While at 80% and 100% impurity, when the edges with each team are

mostly inhibiting and those across teams are mostly activating, we still see a small number of networks showing negative CC AB.

Impurities affect the frequency of pure states and team correlation more than density

After analysing the effect of density and impurity individually, we investigated the combined effect of different impurity and density values on F1 and CC of the TTN networks. We generated 100 networks each for all combinations of density and impurity values - 0%, 20%, 40%, 60%, 100%. At all densities, the networks with 60% or higher impurities show an F1 value of 0, indicating that high impurity can impair the TTN functioning irrespective of density. At 20% impurity, we observe a non-zero mean F1 for all densities as seen earlier (compare **Fig 3A with Fig 2B)**. As density increases, we see an increase in the mean value of F1 for networks with 20% impurity, indicating that density can make the phenotypic output resilient to these impurities. Note that the magnitude of increase in mean F1 is lower from 80% to 100% as compared to other consecutive density points. However, at 100% density, the mean F1 for 20% impurity networks is very similar as that at 0% impurity, while there is a strong decrease in mean F1 for other densities (**Fig 3B)**. This observation indicates that high density prioritizes negating the effects of impurity over adding self-activation to the network. At all other values of density, we see a clear decrease in mean F1 as impurity increases (**Fig 3B**). The median values of F1 (horizontal dashes within the boxplots) follow the same trend as that of the mean. First, we take a closer look at the networks with 20% impurity in **Fig 3B** (orange boxes). The range of F1 values is 0 to 1 for densities 40% to 100%. At 20 and 40% density, a large fraction of the networks have low F1 values. The span of the inter-quartile range (IQR) for F1 decreases from 40% to 100% density. However, the upper limit of the IQR increases from 40 to 80% density, but goes back down at 100% density, reminiscent of the decrease observed in **Fig 1E**. The lower-limit of the IQR consistently increases with increase in the density. We interpret this behaviour in the following manner. On average, increase in density increases F1 while increasing impurity reduces F1. Near the lower limit of the IQR, impurity dominates, while near the upper limit density dominates, evident by the decrease in F1 at 100% density as compared to 80% density. However, other network features can impact this visible competition between impurity and density.

Correlation coefficient reveals further interesting observations in this regard. As seen in **Fig 2B,** the correlation coefficient moves from value close to -1 to a value close to 1 as impurity increases, following a shift in the network structure from mutually inhibiting teams to mutually activating teams **(Fig 3C)**. As the density increases, the range of CC values over the same range of impurity values increases **(Fig 3D).** We found similar dependence of F1 and CC AB on density and impurity for team size of 10 **(Fig S3).** When density is varied at constant values of impurity, the direction of change in correlation coefficient depends on the impurity value **(Fig 3C)**. For impurity less than 50%, we see a decrease in the correlation coefficient (i.e., CC becomes more negative), whereas after 50%, CC increases, becoming more positive. Note that below 50% impurity, mutual inhibition of teams is dominant, while above 50% mutual activation is dominant, possibly explaining the above-mentioned trend. Overall, we find that the increase in density amplifies the impact of the dominant behaviour of the network in terms of correlation coefficient. Thus, unlike in cases of no impurity (**Fig 1F**), we see a clear effect of density on CC in presence of impurities.

While F1 is a strict measure (**Fig S2),** CC AB is more flexible. At 40% impurity, we do not see any networks with an F1 of 1, and a very low fraction of networks with non-zero F1. However, at 40% and 60% impurity values, we see networks with 1 and -1 correlation coefficients at all densities above 20%. While the changes in mean F1 and CC are captured well by the density and impurity

of the TTN networks, the wide range of values suggest that predicting these metrics for individual networks would require additional understanding of the network topology.

To calculate the relative effect of density and impurity on F1 and CC, we generated an ensemble of 2500 TTNs with the density and impurity randomly selected from the range 20-100% and simulated them. We calculated pairwise correlation between the density and the impurity vectors with F1 **(Fig 3E)** and CC **(Fig 3F)** vectors. In other words, we measured the association of each parameter with F1 and CC as the other parameter(s) is varied over the wide range. As expected, impurity has a negative (positive) correlation with F1 (CC AB) while density has a positive (negative) correlation with these metrics correspondingly (**Fig S4A-B)**. We find that impurity has a stronger correlation with both F1 and CC as compared to density, suggesting that impurity has a stronger impact on both these metrics. Because F1 falls to zero after 40% impurity, we studied the networks with impurity $\leq$ 40% separately and found that impurity still has a stronger correlation with both F1 and CCAB than density has. At a constant impurity, the effect of density on CCAB is much lower **(Fig 3C)** as compared to the effect of impurity at a constant density **(Fig 3D)**.

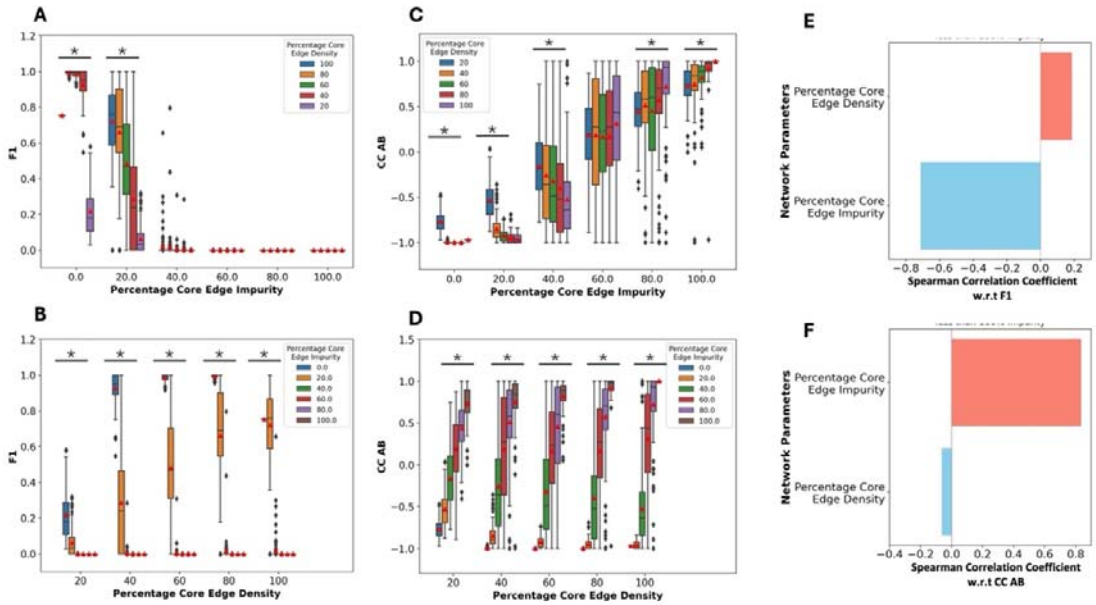

Figure 3: Varying the percentage of impure edges and density together*. Comparison between the distributions of A) F1 and C) CC AB for TTS-5 networks, having the same Percentage Core Edge Impurities but different Percentage Edge Densities. Comparison between the distributions of B) F1 and D) CC AB for TTS-5 networks, having the same Percentage Core Edge Density but different Percentage Edge Impurities. Bar plot depicting the Pearson's correlation coefficient of Network parameters, percentage core edge density and impurity with (E) F1 and (F) CC AB. * indicates that p-value of 1-way ANOVA is < 0.05*

Resilience to global perturbations – interaction of teamed networks with large random networks

One factor often ignored in GRN based models is the interaction of these networks with the rest of the signaling networks within which they are embedded. Indeed, biological networks have

been argued to be modular(Serban 2020; Alcalá-Corona et al. 2021; Kadelka et al. 2023), but multiple phenotypic plasticity programs are interlinked, such as EMT, stemness and drug resistance through few intermediary molecules and pathways(Pasani et al. 2020; Bangarh et al. 2024). Thus, any network reduction strategy in terms of identifying teams of nodes should be capable of recapitulating the effect of such global interactions. We had previously shown that: 1) Toggle switch motifs are resilient to perturbations from such “global” interactions to a large extent (Harlapur et al. 2022). 2) the correlation and PC1 variance of larger networks are significantly affected by the presence of a sub-network with teams (Hari et al. 2025). These observations indicate that teams can provide resilience to global interactions similar to that seen in a toggle switch. Thus, we investigated the effect of global interactions on the phenotypic outcome of TTN.

Network Parameter	**Range**
Percentage Core Edge Density	Feasible Densities > 20%
Percentage Core Edge Impurity	Feasible Impurities > 20%
Mean Connectivity of external network	Mean Connectivity ∈ [2,11]
Average Indegree of Core Node	Average Indegree ∈ {0,1, …. ,19, 20}
Average Outdegree of Core Node	Average Indegree ∈ {0,1, …. ,19, 20}

Table 1: *Ranges for different parameters considered for network embedding*

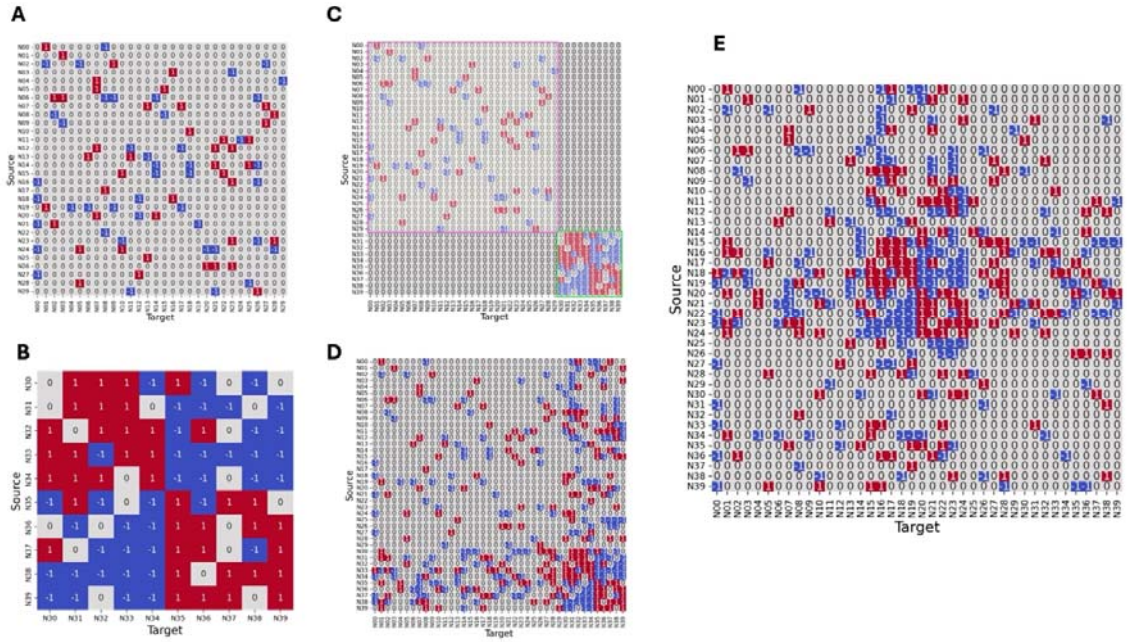

Figure 4: Schematic representing the procedure of embedding core two-team networks in larger external networks*. A) Randomly generated External Network of 30 genes, N00 to N29, having desired Mean Connectivity (MC = 2.8 in A). B) Randomly generated Core Network of 80% Core Edge Density and 20% Density to be embedded, 10 Genes, N30 to N39. C) Bringing together the Core and External Networks. D) Introducing incoming and outgoing edge between the core and external network. E) Centering the core shown in the adjacency matrix D by swapping the names of genes, N15 to N24, with genes N30 to N39.*

We embedded TTNs in a larger external network of 30 nodes, sampling external network parameters from the ranges mentioned in **Table 1** (see schematic in **Figure 4** and **S5**). We investigated three external network parameters that can potentially influence the dynamics of the core network: 1) Mean Connectivity, a measure similar to density that describes the number of connections each node can have within a network on average. 2) Average indegree to the core node, measured as the average number of connections from the external network to the nodes of the core network, and 3) Average outdegree of the core node, measured as the number of edges from the nodes of the core network that can affect the core network dynamics via feedback through the external network and the indegree to the core network. We first generated the core and external network separately. Core network was generated using the stochastic block model as described earlier, varying the core edge density, core edge impurity and team size as required for the particular experiments **(Fig 4A)**. For the external network, we generated a matrix of dimensions 30 X 30 filled with zeros, where each cell represents an edge from the corresponding node in the row to that in the column. We then randomly chose $Mean\ Connectivity * 30$ edges in the matrix, and assigned 1 (activation) or -1 (inhibition) to these edges with equal probability (**Fig 4B)**. We then combined the core and external matrices together as shown in **Fig 4C.** We then added $N * Average\ Indegree$ edges (randomly choosing activations and inhibitions with equal probability) to the top right rectangle that contains the edges from the external network to the core network and $N * Average\ Outdegree$ edges to the bottom left rectangle that contains the edges from the core network to the external network, where N is the number of nodes in the network **(Fig 4D,E)**. Note that the mean connectivity relates to density of the external network as follows:

$$Density_{external} = \frac{Mean\ Connectivity}{30}$$

We refer to the mean connectivity instead of density for external network so that it remains distinct from core edge density. The choice for the range of mean connectivity was inspired from the distributions of connectivity reported for an ensemble of biological networks (Kadelka et al. 2024). We first wanted to test the effect of core network parameters on F1 of an embedded TTN, starting with the team size. We generated 100 such networks for each value of core team size (varying from 1 to 6) with 100% core edge density, 0% core edge impurity and chose the external network parameters randomly from the ranges described in **Table 1.** Apart from team size 2, TTN shows higher mean F1 values than toggle switch when embedded in a larger network **(Fig 5A,** compare team size 1 with higher team sizes**)**. The mean F1 saturates at 1 for team size above 5, suggesting that larger TTN networks are more resilient to external perturbations. This inference was reinforced in CC AB, where the correlation remained strongly negative from team size 2 onwards **(Fig S6A)**. Based on this saturating behaviour and computational costs of simulations, we chose a Team Size of 5 for further embedding experiments such that we are simulating 40 (= 10 + 30) node networks.

Next, we varied the density of the embedded TTN, keeping the size at 5 nodes per team and impurity at 0% and randomly choosing the external network parameters from their corresponding ranges. Similar to the unembedded case, mean F1 increases with increasing density. While the mean F1 reaches 1 around 60% density in unembedded case, it takes 80% density for mean F1 to reach 1 in embedded networks **(Figure 5B)**. Team correlation remained negative for all densities **(Fig S6B).** Interestingly, TTN could only withstand up to an impurity of 20% before losing the F1 frequency, suggesting that internal perturbations affect the phenotypic landscape

more than external perturbations. We similarly explored the effects of core impurity on the embedded TTN landscape (**Figure 5C).** As expected, increased impurity reduces F1, with mean F1 falling to 0 at 40% impurity. At 20% impurity, the variation in F1 increases upon embedding (compare **Fig 2D** with **Fig 5C),** with more networks having a lower value of F1 due to the combined effect of internal and external perturbations to TTN. Similar to the unembedded case, the CC AB values increased with increasing impurity, turning positive at impurities higher than 60% (**Fig S6C).**

We then explored the resilience that TTN networks have to external perturbations by controlling for the variables describing how well the external network is connected to the core network. Previously, we had found the toggle switch to be resilient up to an in-degree of 5 on each of the two nodes. Here, we defined indegree of each node as the average indegree of the nodes of the TTN (for example, if the total number of incoming edges on TTN is 10 for 10 nodes in TTN, the indegree is 1). Note that this definition implies that the indegree of a team from the external network is N times the average indegree of each node, where N is the number of nodes in a team (5 here). We generated TTN embeddings for multiple combinations of values of in-degree and density. For each of these networks, we maintained the mean connectivity of the external networks at 11 to ensure the maximum impact on while randomly sampling average outdegree of core nodes. Interestingly, we find the F1 for TTN at 100% density is resilient to large values of in degrees, with the values of F1 staying at 1 up to in degree of 10, and mean F1 reaching 0.85 at the in degree 20 **(Figure 5D, pink box)**. At lower densities, the effect of indegree could be seen on the decreasing F1 value, as expected. However, TTN proves to be more resilient than a toggle switch to external perturbations even at lower densities. While toggle switch lost the features of bimodality after an indegree of 5, TTN maintained their F1 at a team indegree of 5 (compare average indegree of 1 in **Fig 5D** with **Fig 1E**). A similar effect of indegree and density could be seen (**Fig 5E)** where, as indegree increases, the CC AB increases. Note, however, that CC AB remains negative in all cases, except for a small fraction of networks at 20% density. These results show that the TTN is highly resilient to external perturbations in the absence of impurities.

To better understand the dependence of F1 on the various network parameters studied in this section, we generated 2500 networks with random values of the parameters sampled from the ranges described in **Table 1**, and calculated the F1 values emergent from each network. We then calculated the correlation coefficient between each parameter and the F1 vectors as a measure of the relative dependence of F1 on the metrics. We found that F1 depends strongly on the core impurity, followed by core density, evident from the strength of correlation between the vectors **(Fig 5F)**. Overall, our results suggest that TTN is highly resilient to external perturbations, making its study as an isolated model valid in presence of the global network. Furthermore, TTN has a higher resilience than toggle switch for external perturbations.

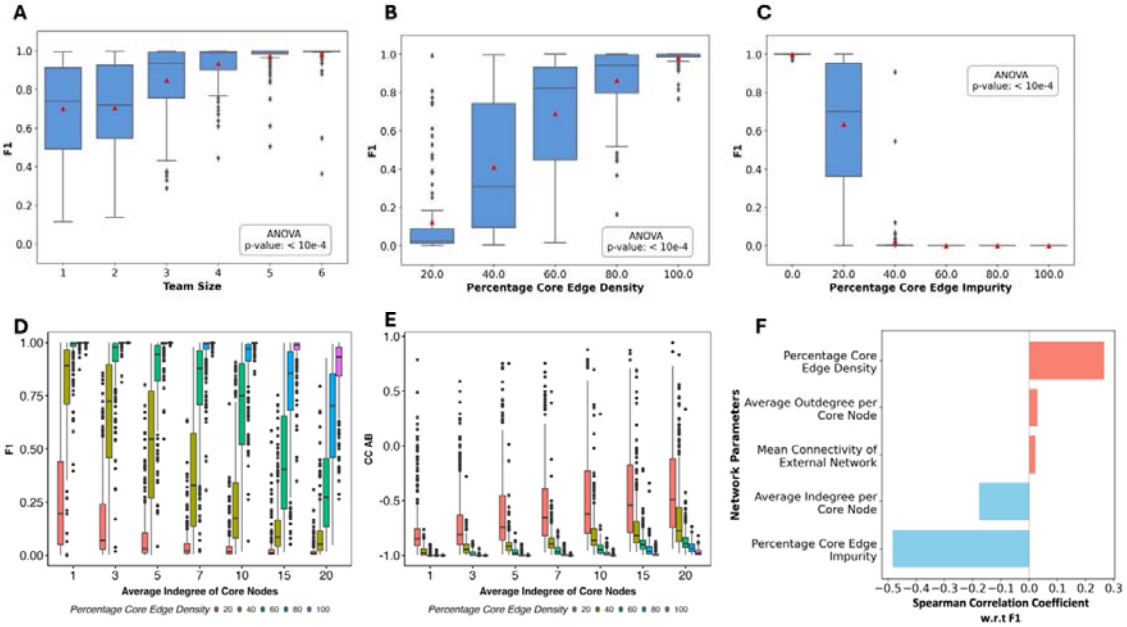

Figure 5: Dynamics of Embedded Teamed Toggle Switch Networks. Boxplots comparing the Distributions of F1 *for variation in A) Team Size, B) Percentage Core Edge Density, C) Percentage Core Edge Impurity, and D) Average Indegree per Node of a Team of fully connected TTS-5 networks embedded in a 30 Gene External networks. Bar plot showing the Pearson's correlation coefficient of F1 with Percentage Core Edge Density, Impurity, Mean Connectivity of External Network, Average Indegree per Core Node and Average Outdegree per Core Node. * Indicates p-value < 0.05. Results of 1-way ANOVA indicated on the plot.*

Discussion

Network coarse-graining is a common practice when dealing with large-scale networks, often involving the replacement of a group of nodes with a single “super” node, based on features such as positive feedback and strong connectedness and communities (Erban et al. 2006; Saadatpour et al. 2013; Snowden et al. 2017; Caranica and Lu 2023; Kadelka et al. 2023). Inferring gene regulatory networks from perturbation time-course experimental data also allows identifying such coarse-grained structures(Wang et al. 2009; Sarmah et al. 2022). Binary cell fate decision systems are often modelled using toggle switches, serving as coarse grained approximations of much larger networks comprising of numerous transcription factors corresponding to each of the two cell fates(Roeder and Glauche 2006; Zhou and Huang 2011; Okawa et al. 2016). Indeed, simulations of corresponding large scale networks wherever available do support the approximation as a toggle switch qualitatively in terms of predominant phenotypes (Ríos et al. 2015; Udyavar et al. 2017; Font-Clos et al. 2018). However, studies pertaining to the topological features of large networks that allow for a quantitatively valid coarse-graining of large-scale networks are missing in the current literature. In this study, we try to fill that gap by comparing the phenotypic outputs of “teams of nodes” with those emergent from a toggle switch.

Teams are a topological feature of binary cell-fate decision networks that we have observed in multiple biological contexts (Chauhan et al. 2021; Pillai and Jolly 2021; Shyam et al. 2023; Sehgal et al. 2024; Hari et al. 2025). The “influence matrix” representation of these networks had revealed two communities that are identified by groups of nodes with positive influence within

themselves and negative influence across, forming a “Teamed-Toggle-Switch” (TTN) (Chauhan et al. 2021; Hari et al. 2022b). This influence is mediated through both direct and indirect interactions between each pair of nodes. An intuitive coarse graining of the influence matrix leads to a toggle switch of two hypernodes with each hypernode representing one team. However, we find here that such coarse graining of these networks is not always appropriate.

We studied three key features of the TTN : the size of each team, density of the network and impure edges that have the opposite nature as appropriate for the team classification (i.e. inhibitions within teams and activations across teams). We used the total frequency of pure states (expression of nodes belonging to one team is on, while that of the other team is of) and the average correlation across nodes of the network as representatives of the phenotypic landscape. While the correlation coefficient is a low-resolution measure of the mutual inhibition between the teams, F1 is a more nuanced metric describing how often can these networks give rise to “hybrid” phenotypes, as opposed to two dominant cell fates that the network is supposed to give rise to.

The correlation coefficient remained strongly negative for different values of team sizes and densities. With increasing impurities, the correlation coefficient increased, turning positive for impurity values above 50%. This behaviour is explained by the fact that above 50% impurity, the “pure” phenotypes are destabilised, while “all or none” phenotypes are stabilized. These results suggest the estimation of transcriptional networks using correlation between the nodes may not be appropriate. At 40% and 60% impurities even at high density, we see networks with team correlation of -1 and 1. Note that the team structure is nearly randomized at these impurity values. This result indicates the possibility of observing strong correlation between groups of genes in transcriptomic data, despite there not being any consistent mechanistic reason for the same.

F1 also proved to be less sensitive to team size, but increased with density and reduced with impurity. The F1 value for a toggle switch is 1 with Boolean simulations, and near 0.8 with continuous simulations. In both cases, we find that the TTN needs a density of 60% or more to reach the corresponding F1 value of the TS. Furthermore, impurities more than 20% lead to a sharp decrease in F1. Putting these results in perspective, we note that biological networks that we have studied in previous studies have a density of around 20-30% and impurities less than 20% (Hari et al. 2025). At these values, the mean F1 is low. However, these are also regions where there is a large variation in the F1 values, with the possibility of networks having both high and low F1 values. Interestingly, TTN showed a higher resilience than TS to external perturbations. The phenotypic landscape emergent from TTN is more sensitive to internal parameters than it is to the properties of the external network.

Increasing density has interesting effects on different metrics. F1 increases with density up to 80%, but decreases at a 100% density, a behaviour observed in both Boolean and continuous simulation formalisms. However, in presence of impurity and external perturbations, F1 monotonically increases with density. Furthermore, density amplifies the effect of the dominant network structure in correlation coefficient, as seen in the impurity experiments. Below 50% impurity, the correlation coefficient becomes more negative with increasing density, whereas above 50%, the correlation becomes positive.

The internal properties such as density and impurity were able to explain the trends of mean F1 and CC well, but failed to explain the occurrence of some exceptions, especially in the presence of impurity. Even at 100% impurity, we found some networks with a team correlation of -1. Similarly at 40% impurity where the interactions are nearly random, we find networks with high values of F1. Explaining such apparent anomalies would potentially invoke including additional

topological features in the network such as node connectivity measures (Wang et al. 2022), strongly connected components, stable motifs (Zañudo and Albert 2013) and network redundancy (Gates et al. 2021).

Our analysis of network embedding further provides key insights into how cell-fate decision systems can be dynamically modular (Deritei et al. 2016). Even at lower densities, we found that the dynamics of TTN are resilient to the influence of external network. Together with our previous results on the robust low-dimensionality of TTNs, we propose teams as an underlying mechanism for modular dynamics of phenotypic switches, such that they maintain their phenotypes when interacting with other switches/signalling networks in the cell.

We made multiple assumptions in the current study, which would require careful considerations in the future studies of the topic. First, we simulated these networks majorly using a threshold-based Boolean formalism. While threshold based formalisms that are often employed in modelling Gene regulatory networks (Mendoza and Alvarez-Buylla 1998; Li et al. 2004; Font-Clos et al. 2018), they cannot account for the logical rules and interaction parameters that govern the emergent dynamics (Zañudo et al. 2011). Second, we assumed that both teams have equal sizes. While this is not an issue with the threshold-based formalism used to simulate the networks here, a different simulation formalism might lead to asymmetry in the phenotypic landscape caused by the difference in team sizes. However, this might not matter for F1, as the metric measures the extent of pure states and does not distinguish between the pure states emergent from the system. Similar symmetry was maintained while constructing the networks, making sure that each of the four submatrices of the interaction matrix defined by the team structure have near identical properties. Investigating the effect of these asymmetries on the phenotypic landscape will be the focus of future studies.

Despite the structural similarities between TTN and toggle switch, we have shown here that approximating TTN as a TS is not valid even when using a simple and symmetric simulation formalism as the one used here. While high density is required for TTN to have qualitatively similar properties as TS, phenotypic landscape emergent from TTN are strongly resilient to external perturbations, thereby making it more independent and robust than a simple TS. Furthermore, as any network can be visualized as a two team network with some density and impurity. Hence, our current results allow us to predict the dynamical features of the phenotypic landscape emergent from any network to a reasonable extent.

Methods

Simulating Networks using Boolean formalism

We simulated the TTNs primarily using a threshold based Boolean formalism. Each gene in the network can take one of 2 states: +1 corresponding to high expression and -1 corresponding to low expression, We define a state vector S(t) to be a vector composed of states of each gene part of the network at time ‘t’. If the network is composed of ‘N’ genes, then the state vectors is composed of ‘N’ elements, each representing the state of a gene. Following the update rule, the state is of the system updates via discrete transitions.

Update Rule:

Adj is the Adjacency Matrix, in which the row indices are the Targer Genes, and the column indices are the Target Genes.Adj_{ij} represents the interaction from the source gene ‘j’ to target genes ‘i’.
S(t) is the state vector at time ‘t’. $S_i(t)$ is the state of gene ‘i’

$$s_i(t+1) = \begin{cases} +1, \sum_j Adj_{ij} s_j(t) > 0 \\ -1, \sum_j Adj_{ij} s_j(t) < 0 \\ s_i(t), \sum_j Adj_{ij} s_j(t) = 0 \end{cases}$$

Where only one gene 'i' is randomly selected and updated at each time step.

We simulate the network starting at 100000 random state vectors. Each random state is updated using the dynamics given above until a steady state (i.e., S(t+1) = S(t)) is reached. The final state achieved from the simulation is then analysed.

Here, we follow the Asynchronous Update Rule, by which at each time step a single gene is selected at random and its state is updated. To check whether a steady state has been reached, we used synchronous update.

Metrics

F1 – Fraction of Pure States

A "pure" is defined as a steady-state in which that genes belonging to one team have high expression and those belonging to the other team have low expression. F1 is defined as the ration of total number of Pure States to total number of steady states. In the case of embedded networks, the pure states were calculated with respect to gene teams of the core.

CC AB – Correlation Coefficient between Average Expressions of Team A & B

The average expression of genes in Team A (Team A_{Avg}) and average expression of genes in Team B (Team B_{Avg}) were calculated for each steady state. The CC AB was then calculated as the spearman correlation coefficient was found for Team A_{Avg} vs Team B_{Avg}.

Generating artificial networks with different values of density, size and impurity

Artificial networks are generated using the stochastic block model (Holland et al. 1983), with constant probability of edges in all blocks of a network. The block model allows us assign team configurations. In TTN, the four blocks belong to two within team interactions and two across teams interactions. We first generate four blocks of size NXN each where N is the size of each team. Then, within each block, we add edges weighted according to the nature of the block (1 in within team interactions and -1 in across team interactions) with probability $\frac{d}{100}$ where d is the desired percentage density. We then change the weights of each edge with a probability $\frac{i}{100}$, where "i" is the desired percentage impurity of the network. To investigate the effect of specific core and external network parameters, we generated Networks as follows.

Core Network

For Generating Core Networks with varying Edge Density, as per the density required, the number of Edges that need to be removed per quadrant of the core adjacency matrix (Adj) was decided as follows:

$$Edges\ to\ be\ removed\ per\ quadrant = int((1 - Required\ core\ density) * 25)$$

From each quadrant, the specific number of edges was removed. So, the total number of edges in each quadrant is the same, i.e. the total number incoming of positive and negative interactions to one team is the same as the other. This was done to ensure that asymmetry in the number of edges doesn't skew our initial experiments.

For the addition of impurity, networks of their respective densities are taken as input. Based on the required percentage edge impurity, the number of edges to be flipped from activation to inhibition and vice versa is decided as follows.

$$Edges\ to\ be\ flipped\ per\ quadrant = int(Total\ edges\ per\ quadrant * Required\ Impurity)$$

And in every quadrant, the same number of pure edges are flipped impure ones

Generating the External Network of a specific Mean Connectivity

Throughout our experiments, we have maintained a fixed size of 30 Genes for the external network. The total number of edges in the external network is determined based on the desired value of Mean Connectivity.

In the experiments to determine the effect of variation in the Mean Connectivity of the external Network, the Mean Connectivity was strictly controlled. In all other simulation experiments, the Mean Connectivity (m) parameter ranged between 2 and 12 for the external network.

Hence on average, every external node has **'m'** incoming/outgoing interactions. To achieve this, we first generate 30X30 matrix of zeroes, randomly select m*30 positions in the matrix and assigns 1 or -1 to these positions with equal probability, thereby ensuring an equal number of activations and inhibitions on average.

Connecting the Core Network and the External Network

Now we have an external Network of 30 Genes and a Two team-network Core Network of 10 Genes (5 Genes Per Team). While connecting the External and Core Networks, the key parameters considered are the indegree and outdegree per Team.

Indegree

For a given value of indegree per gene in a team (i), it was ensured that, on average, each gene in each team had an indegree of (i). Furthermore, the indegree of each team was kept exactly the same. (Figure 4).

Outdegree

Similarly, for a given value of outdegree per gene in a team (o), it was ensured that, on average, each gene in each team had an average outdegree of (o). And the outdegree of each team was kept exactly the same.

Frustration

For a give state (S) of the network, an edge ($j \rightarrow i$) is frustrated if $Adj_{ij}s_is_j < 0$. The frustration of the state is then defined as the fraction of frustrated edges in the network corresponding to that state. In the core TTNs generated in this manuscript, the frustration of a pure state is zero in absence of any impurities, since nodes within the same team have the same sign, i.e., $s_i * s_j > 0$ and the corresponding edge, if exists, will be positive ($Adj_{ij} \geq 0$). Similarly, for nodes belonging

to different teams, $s_i * s_j < 0 \; and \; Adj_{ij} \leq 0$. Thus, $Adj_{ij} s_i s_j \geq 0$ for all (i, j) in absence of impurities. In presence of impurities, the only frustrated edges for pure states will be the impure edges, making the frustration of pure states equal to the fraction of impure edges in the network.

Data and Code availability

The raw data files (network files, steady state frequency files) are available with the corresponding authors upon reasonable request. Processed data used to generate figures and codes to generate the networks and analyse the raw data has been deposited in the GitHub repository at https://github.com/saishyam1/Resilience_of_Teams.

Author Contributions

SS and NN performed analysis and data analysis, MKJ and KH conceptualized and supervised research. MKJ received funding. All authors contributed to writing and editing the manuscript.

Funding

MKJ was supported by Param Hansa Philanthropies. SS was supported by the Kishore Vaigyanik Protsahan Yojana (KVPY) Fellowship, Government of India. KH was supported by Prime Ministers' Research Fellowship (PMRF), Government of India.

Conflict of Interest

The authors declare no conflict of interest.

References

Alcalá-Corona SA, Sandoval-Motta S, Espinal-Enríquez J, Hernández-Lemus E (2021) Modularity in Biological Networks. Front Genet 12:701331. https://doi.org/10.3389/FGENE.2021.701331

Arthur TD, Nguyen JP, D'Antonio-Chronowska A, et al (2024) Complex regulatory networks influence pluripotent cell state transitions in human iPSCs. Nature Communications 2024 15:1 15:1–19. https://doi.org/10.1038/s41467-024-45506-6

Bangarh R, Saini R V., Saini AK, et al (2024) Dynamics of epithelial–mesenchymal plasticity driving cancer drug resistance. Cancer Pathogenesis and Therapy. https://doi.org/10.1016/J.CPT.2024.07.002

Brabletz S, Brabletz T (2010) The ZEB/miR-200 feedback loop—a motor of cellular plasticity in development and cancer? EMBO Rep 11:670. https://doi.org/10.1038/EMBOR.2010.117

Caranica C, Lu M (2023) A data-driven optimization method for coarse-graining gene regulatory networks. iScience 26:105927. https://doi.org/10.1016/J.ISCI.2023.105927

Celià-Terrassa T, Bastian C, Liu D, et al (2018) Hysteresis control of epithelial-mesenchymal transition dynamics conveys a distinct program with enhanced metastatic ability. Nature Communications 2018 9:1 9:1–12. https://doi.org/10.1038/s41467-018-07538-7

Chauhan L, Ram U, Hari K, Jolly MK (2021) Topological signatures in regulatory network enable phenotypic heterogeneity in small cell lung cancer. Elife 10:. https://doi.org/10.7554/elife.64522

Cinquin O, Demongeot J (2002) Roles of positive and negative feedback in biological systems. C R Biol 325:1085–1095. https://doi.org/10.1016/S1631-0691(02)01533-0

Deritei D, Aird WC, Ercsey-Ravasz M, Regan ER (2016) Principles of dynamical modularity in biological regulatory networks. Scientific Reports 2016 6:1 6:1–19. https://doi.org/10.1038/srep21957

Dublanche Y, Michalodimitrakis K, Kümmerer N, et al (2006) Noise in transcription negative feedback loops: simulation and experimental analysis. Mol Syst Biol 2:41. https://doi.org/10.1038/MSB4100081

Erban R, Kevrekidis IG, Adalsteinsson D, Elston TC (2006) Gene regulatory networks: A coarse-grained, equation-free approach to multiscale computation. Journal of Chemical Physics 124:. https://doi.org/10.1063/1.2149854/349155

Font-Clos F, Zapperi S, Porta CAM La (2018) Topography of epithelial–mesenchymal plasticity. Proceedings of the National Academy of Sciences 115:5902–5907. https://doi.org/10.1073/PNAS.1722609115

Gardner TS, Cantor CR, Collins JJ (2000) Construction of a genetic toggle switch in Escherichia coli. Nature 403:339–342. https://doi.org/10.1038/35002131

Gates AJ, Correia RB, Wang X, Rocha LM (2021) The effective graph reveals redundancy, canalization, and control pathways in biochemical regulation and signaling. Proc Natl Acad Sci U S A 118:e2022598118. https://doi.org/10.1073/PNAS.2022598118/SUPPL_FILE/PNAS.2022598118.SAPP.PDF

Gupta PB, Pastushenko I, Skibinski A, et al (2019) Phenotypic plasticity as a driver of cancer formation, progression and resistance to therapy. Cell Stem Cell 24:65. https://doi.org/10.1016/J.STEM.2018.11.011

Hari K, Harlapur P, Gopalan A, et al (2022a) Emergent properties of coupled bistable switches. J Biosci 47:1–15. https://doi.org/10.1007/S12038-022-00310-6/FIGURES/5

Hari K, Harlapur P, Saxena A, et al (2025) Low dimensionality of phenotypic space as an emergent property of coordinated teams in biological regulatory networks. iScience 0:111730. https://doi.org/10.1016/J.ISCI.2024.111730

Hari K, Sabuwala B, Subramani BV, et al (2020) Identifying inhibitors of epithelial–mesenchymal plasticity using a network topology-based approach. npj Systems Biology and Applications 2020 6:1 6:1–12. https://doi.org/10.1038/s41540-020-0132-1

Hari K, Ullanat V, Balasubramanian A, et al (2022b) Landscape of epithelial–mesenchymal plasticity as an emergent property of coordinated teams in regulatory networks. Elife 11:. https://doi.org/10.7554/eLife.76535

Harlapur P, Duddu AS, Hari K, et al (2022) Functional Resilience of Mutually Repressing Motifs Embedded in Larger Networks. Biomolecules 12:1842. https://doi.org/10.3390/BIOM12121842/S1

Holland PW, Blackmond K, Leinhardt S (1983) STOCHASTIC BLOCKMODELS: FIRST STEPS * Educational Testing Seroice **. Soc Networks 5:9–137

Huang B, Jia D, Feng J, et al (2018) RACIPE: a computational tool for modeling gene regulatory circuits using randomization. BMC Syst Biol 12:74. https://doi.org/10.1186/s12918-018-0594-6

Huang B, Lu M, Jia D, et al (2017) Interrogating the topological robustness of gene regulatory circuits by randomization. PLoS Comput Biol 13:e1005456. https://doi.org/10.1371/JOURNAL.PCBI.1005456

Jaruszewicz J, Lipniacki T (2013) Toggle switch: noise determines the winning gene. Phys Biol 10:35007. https://doi.org/10.1088/1478-3975/10/3/035007

Jolly MK, Preca B-T, Tripathi SC, et al (2018) Interconnected feedback loops among ESRP1, HAS2, and CD44 regulate epithelial-mesenchymal plasticity in cancer. APL Bioeng 2:031908. https://doi.org/10.1063/1.5024874

Jopling C, Boue S, Belmonte JCI (2011) Dedifferentiation, transdifferentiation and reprogramming: three routes to regeneration. Nature Reviews Molecular Cell Biology 2011 12:2 12:79–89. https://doi.org/10.1038/nrm3043

Kadelka C, Butrie TM, Hilton E, et al (2024) A meta-analysis of Boolean network models reveals design principles of gene regulatory networks. Sci Adv 10:822. https://doi.org/10.1126/SCIADV.ADJ0822/SUPPL_FILE/SCIADV.ADJ0822_DATA_S1_TO_S5.ZIP

Kadelka C, Wheeler M, Veliz-Cuba A, et al (2023) Modularity of biological systems: a link between structure and function. J R Soc Interface 20:. https://doi.org/10.1098/RSIF.2023.0505

Kalra RS, Dhanjal JK, Das M, et al (2021) Cell Transdifferentiation and Reprogramming in Disease Modeling: Insights into the Neuronal and Cardiac Disease Models and Current Translational Strategies. Cells 10:. https://doi.org/10.3390/CELLS10102558

Lai X, Wolkenhauer O, Vera J (2016) Understanding microRNA-mediated gene regulatory networks through mathematical modelling. Nucleic Acids Res 44:6019–6035. https://doi.org/10.1093/NAR/GKW550

Li F, Long T, Lu Y, et al (2004) The yeast cell-cycle network is robustly designed. Proc Natl Acad Sci U S A 101:4781–4786. https://doi.org/10.1073/PNAS.0305937101/SUPPL_FILE/05937FIG7.JPG

Lu M, Jolly MK, Levine H, et al (2013) MicroRNA-based regulation of epithelial-hybrid-mesenchymal fate determination. Proc Natl Acad Sci U S A 110:18144–18149. https://doi.org/10.1073/pnas.1318192110

Mendoza L, Alvarez-Buylla ER (1998) Dynamics of the Genetic Regulatory Network forArabidopsis thalianaFlower Morphogenesis. J Theor Biol 193:307–319. https://doi.org/10.1006/JTBI.1998.0701

Mills JC, Stanger BZ, Sander M (2019) Nomenclature for cellular plasticity: are the terms as plastic as the cells themselves? EMBO J 38:. https://doi.org/10.15252/EMBJ.2019103148/ASSET/035177EB-4B37-4EDC-B3D5-45EBBA3B67E3/ASSETS/GRAPHIC/EMBJ2019103148-FIG-0001-M.PNG

Okawa S, Nicklas S, Zickenrott S, et al (2016) A Generalized Gene-Regulatory Network Model of Stem Cell Differentiation for Predicting Lineage Specifiers. Stem Cell Reports 7:307. https://doi.org/10.1016/J.STEMCR.2016.07.014

Pasani S, Sahoo S, Jolly MK (2020) Hybrid E/M Phenotype(s) and Stemness: A Mechanistic Connection Embedded in Network Topology. J Clin Med 10:60. https://doi.org/10.3390/jcm10010060

Pastushenko I, Blanpain C (2019) EMT Transition States during Tumor Progression and Metastasis. Trends Cell Biol 29:212–226. https://doi.org/10.1016/J.TCB.2018.12.001

Peiró S, Escrivà M, Puig I, et al (2006) Snail1 transcriptional repressor binds to its own promoter and controls its expression. Nucleic Acids Res 34:2077. https://doi.org/10.1093/NAR/GKL141

Pérez-González A, Bévant K, Blanpain C (2023) Cancer cell plasticity during tumor progression, metastasis and response to therapy. Nature Cancer 2023 4:8 4:1063–1082. https://doi.org/10.1038/s43018-023-00595-y

Pillai M, Jolly MK (2021) Systems-level network modeling deciphers the master regulators of phenotypic plasticity and heterogeneity in melanoma. iScience 24:103111. https://doi.org/10.1016/J.ISCI.2021.103111

Ríos O, Frias S, Rodríguez A, et al (2015) A Boolean network model of human gonadal sex determination. Theor Biol Med Model 12:26. https://doi.org/10.1186/S12976-015-0023-0

Roeder I, Glauche I (2006) Towards an understanding of lineage specification in hematopoietic stem cells: a mathematical model for the interaction of transcription factors GATA-1 and PU.1. J Theor Biol 241:852–865. https://doi.org/10.1016/J.JTBI.2006.01.021

Saadatpour A, Albert R, Reluga TC (2013) A REDUCTION METHOD FOR BOOLEAN NETWORK MODELS PROVEN TO CONSERVE ATTRACTORS. SIAM J Appl Dyn Syst 12:1997–2011. https://doi.org/10.1137/13090537X

Sarmah D, Smith GR, Bouhaddou M, et al (2022) Network inference from perturbation time course data. npj Systems Biology and Applications 2022 8:1 8:1–18. https://doi.org/10.1038/s41540-022-00253-6

Sehgal M, Nayak SP, Sahoo S, et al (2024) Mutually exclusive teams-like patterns of gene regulation characterize phenotypic heterogeneity along the noradrenergic-mesenchymal axis in neuroblastoma. Cancer Biol Ther 25:. https://doi.org/10.1080/15384047.2024.2301802

Serban M (2020) Exploring modularity in biological networks. Philosophical Transactions of the Royal Society B 375:. https://doi.org/10.1098/RSTB.2019.0316

Shiraishi T, Matsuyama S, Kitano H (2010) Large-Scale Analysis of Network Bistability for Human Cancers. PLoS Comput Biol 6:e1000851. https://doi.org/10.1371/JOURNAL.PCBI.1000851

Shyam S, Ramu S, Sehgal M, Jolly MK (2023) A systems-level analysis of the mutually antagonistic roles of RKIP and BACH1 in dynamics of cancer cell plasticity. J R Soc Interface 20:. https://doi.org/10.1098/RSIF.2023.0389

Snowden TJ, van der Graaf PH, Tindall MJ (2017) Methods of Model Reduction for Large-Scale Biological Systems: A Survey of Current Methods and Trends. Bull Math Biol 79:1449–1486. https://doi.org/10.1007/S11538-017-0277-2/FIGURES/1

Subbalakshmi AR, Sahoo S, Biswas K, Jolly MK (2022) A Computational Systems Biology Approach Identifies SLUG as a Mediator of Partial Epithelial-Mesenchymal Transition (EMT). Cells Tissues Organs 211:689–702. https://doi.org/10.1159/000512520

Tian T, Burrage K (2006) Stochastic models for regulatory networks of the genetic toggle switch. Proc Natl Acad Sci USA 103:8372–8377. https://doi.org/10.1073/pnas.0507818103

Tripathi S, Kessler DA, Levine H (2020) Biological Networks Regulating Cell Fate Choice Are Minimally Frustrated. Phys Rev Lett 125:088101. https://doi.org/10.1103/PHYSREVLETT.125.088101/FIGURES/4/MEDIUM

Udyavar AR, Wooten DJ, Hoeksema M, et al (2017) Novel Hybrid Phenotype Revealed in Small Cell Lung Cancer by a Transcription Factor Network Model That Can Explain Tumor Heterogeneity. Cancer Res 77:1063–1074. https://doi.org/10.1158/0008-5472.CAN-16-1467

Vandamme N, Denecker G, Bruneel K, et al (2020) The EMT transcription factor ZEB2 promotes proliferation of primary and metastatic melanoma while suppressing an invasive, mesenchymal-like phenotype. Cancer Res 80:2983–2995. https://doi.org/10.1158/0008-5472.CAN-19-2373/654219/AM/THE-EMT-TRANSCRIPTION-FACTOR-ZEB2-PROMOTES

Wang M, Wang H, Zheng H (2022) A Mini Review of Node Centrality Metrics in Biological Networks. International Journal of Network Dynamics and Intelligence 99–110. https://doi.org/10.53941/IJNDI0101009

Wang Y, Wang G, Yang B, et al (2009) Reconstruct gene regulatory network using slice pattern model. BMC Genomics 10:S2. https://doi.org/10.1186/1471-2164-10-S1-S2

Zañudo JGT, Albert R (2013) An effective network reduction approach to find the dynamical repertoire of discrete dynamic networks. Chaos 23:. https://doi.org/10.1063/1.4809777/135853

Zañudo JGT, Aldana M, Martínez-Mekler G (2011) Boolean Threshold Networks: Virtues and Limitations for Biological Modeling. Intelligent Systems Reference Library 11:113–151. https://doi.org/10.1007/978-3-642-19621-8_6

Zhang H, Chen Y, Chen Y (2012) Noise Propagation in Gene Regulation Networks Involving Interlinked Positive and Negative Feedback Loops. PLoS One 7:e51840. https://doi.org/10.1371/JOURNAL.PONE.0051840

Zhou JX, Huang S (2011) Understanding gene circuits at cell-fate branch points for rational cell reprogramming. Trends Genet 27:55–62. https://doi.org/10.1016/J.TIG.2010.11.002

Supplementary Figures

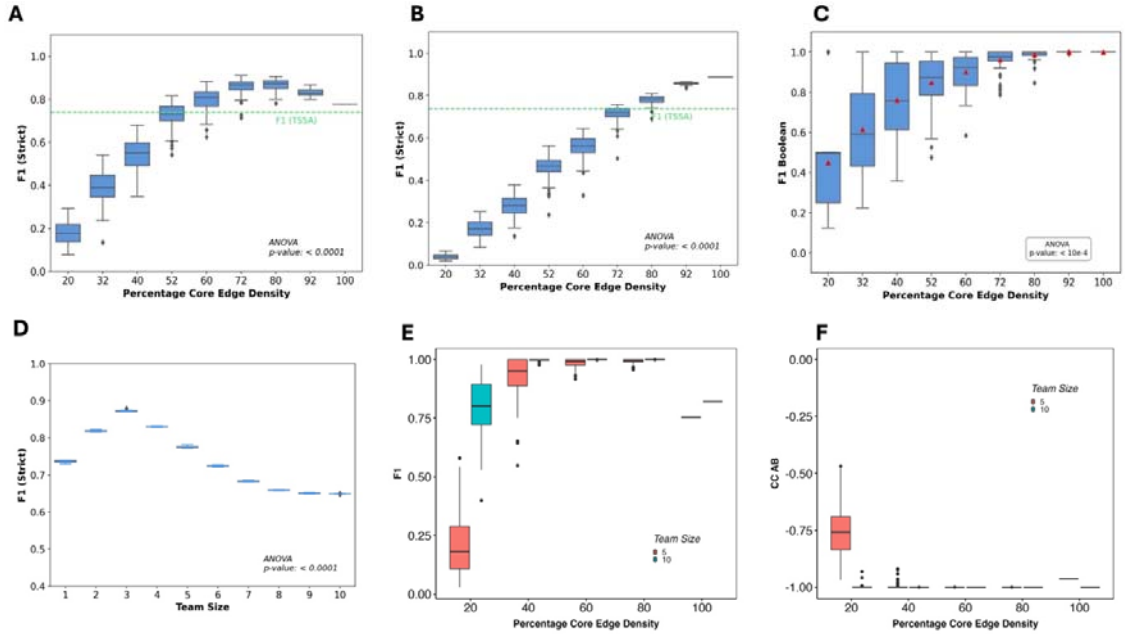

Figure S1*: Change in F1 and CC AB as a function of density and team size. A) Change in F1 calculated using RACIPE with change in TTN density. B) Same as A but for TTN without self-*

activation C) Same as B but for Boolean simulations D) Change in RACIPE F1 as a function of team size for 100% density TTN. E-F) F1 and CC AB with changing densities of TTN from Boolean simulations, for team sizes 5 and 10.

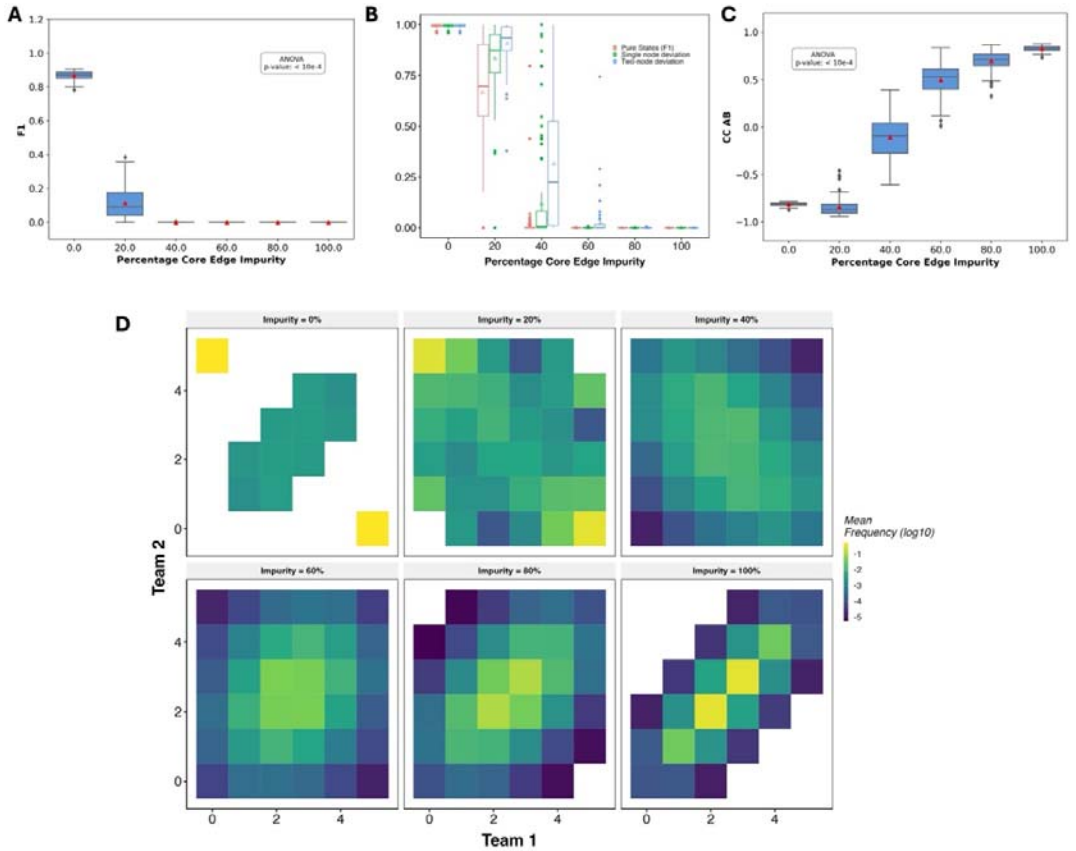

***Figure S2**: Distributions of A) F1 and B) Relaxed F1 metrics and C) CC AB for TTS Core networks with different values for Percentage Core Edge Impurity. D) Heatmap depicting the frequency landscape of Team A Score to Team B Score, for Networks of 80% Core Edge Density and different values percentage core edge impurity.*

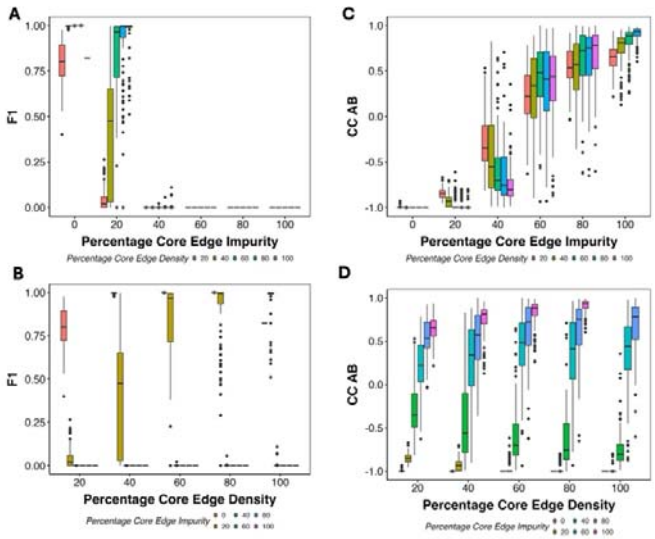

Figure S3*: Effect of Density and Impurity on F1 and CC AB of 20 node TTN. A-B Change in F1 with varying density and impurity. C-D Change in CC AB with varying density and impurity*

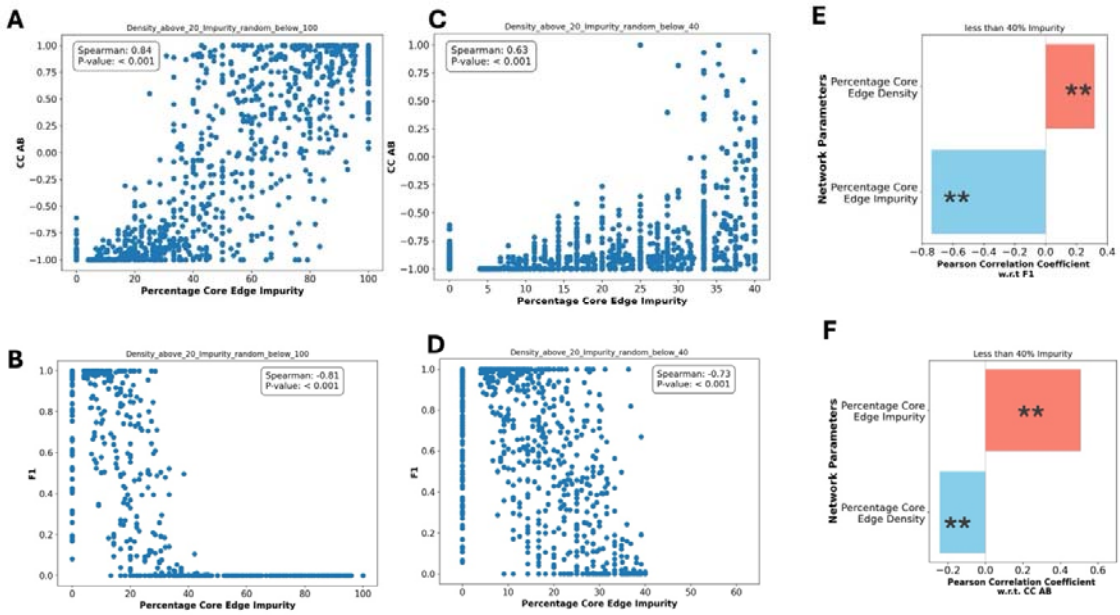

Figure S4*: Scatter plot of Percentage Core Edge Impurity vs A) CC AB and B) F1 of the corresponding network, for Networks with Core Edge Density greater than 20% and Impurity less than 40%. Scatter plot of Percentage Core Edge Impurity vs C) CC AB and D) F1 of the corresponding network, for Networks with Core Edge Density greater >= 20% and Impurity <= 100%. Scatter plot of log(Team Strength) vs F1 of corresponding network for Networks with 80% Core Edge Density and Impurity <= 100%. Box Plots representing the Pearson's Correlation coefficient of Network Parameters, Percentage Core Edge Density and Impurity with respect to E) F1 and F) CC AB. ** indicates that p-value of t-test < 0.05.*

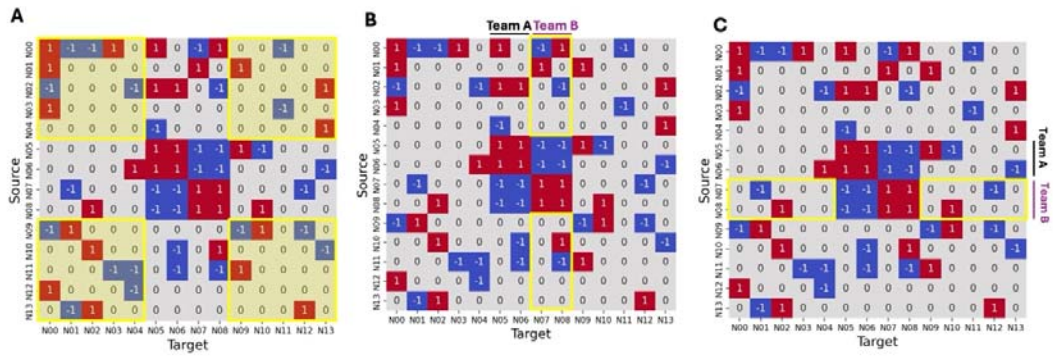

$$\textbf{Mean Connectivity of Peripheral Network} = \frac{\textit{Total Interactions Among Peripheral Genes}}{\textit{Number of Peripheral Genes}}$$

$$\textit{Total Number of Genes in Team B} = G_B$$

$$\textbf{Average Indegree per Gene}_{\textit{Team B}} = \frac{\textit{Indegree of the Team B}}{G_B}$$

$$\textbf{Average Outdegree per Gene}_{\textit{Team B}} = \frac{\textit{Outdegree of the Team B}}{G_B}$$

Figure S5: *Schematic depicting key network parameters investigated in TTS embedded Networks. In the schematic a TTS-2 is embedded in a 10 Gene External Network. A) Yellow Boxes indicate the interactions between external genes. Mean Connectivity is calculated as the ratio of total interactions among external genes to total number of external genes. In B) the Yellow Box highlights the incoming edges to Team B, i.e. Indegree of Team B. The average indegree per gene of a Team is calculated as the ratio of total number of incoming interactions towards genes in the team to the number of genes in the team. In C) the Yellow Box highlights the outcoming edges to Team B, i.e. Outdegree of Team B. The average indegree per gene of a Team is calculated as the ratio of total number of outgoing interactions from genes in the team to the number of genes in the team.*

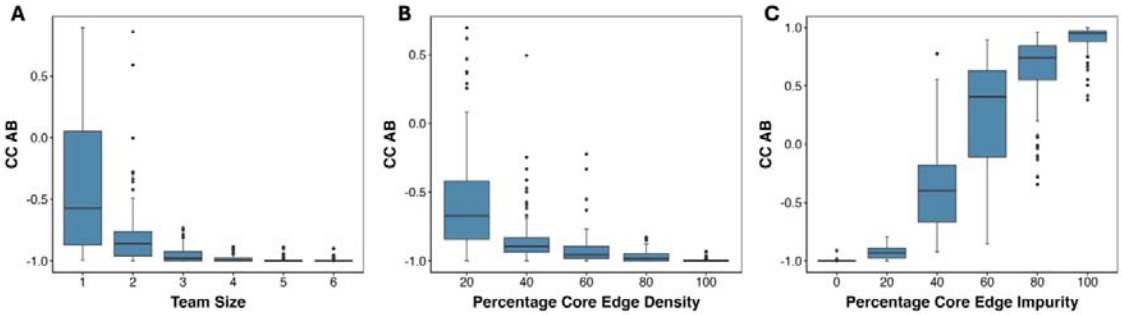

Figure S6: *CCAB as a function of the A) Team Size, B) Density and C) Impurity for embedded TTNs.*